J. Fluid Mech. (2009), *vol.* 641, *pp.* 157–167.
doi:10.1017/S0022112009991959

Turbulent Rayleigh–Bénard convection for a Prandtl number of 0.67

GUENTER AHLERS[1]†, EBERHARD BODENSCHATZ[2], DENIS FUNFSCHILLING[3] AND JAMES HOGG[1]

[1]Department of Physics, University of California, Santa Barbara, CA 93106, USA

[2]Max Planck Institute for Dynamics and Self-Organization, Am Fassberg 17, D-37077 Goettingen, Germany

[3]LSGC CNRS–GROUPE ENSIC, BP 451, 54001 Nancy Cedex, France

(Received 29 July 2009; revised 2 September 2009; accepted 3 September 2009; first published online 23 November 2009)

For the Rayleigh-number range $10^7 \lesssim Ra \lesssim 10^{11}$ we report measurements of the Nusselt number Nu and of properties of the large-scale circulation (LSC) for cylindrical samples of helium gas (Prandtl number $Pr = 0.674$) that have aspect ratio $\Gamma \equiv D/L = 0.50$ (D and L are the diameter and the height respectively) and are heated from below. The results for Nu are consistent with recent direct numerical simulations. We measured the amplitude δ of the azimuthal temperature variation induced by the LSC at the sidewall, and the LSC circulation-plane orientation θ_0, at three vertical positions. For the entire Ra range the LSC involves a convection roll that is coherent over the height of the system. However, this structure frequently collapses completely at irregular time intervals and then reorganizes from the incoherent flow. At small δ the probability distribution $p(\delta)$ increases linearly from zero; for $\Gamma = 1$ and $Pr = 4.38$ this increase is exponential. No evidence of a two-roll structure, with one above the other, was observed. This differs from recent direct numerical simulations for $\Gamma = 0.5$ and $Pr = 0.7$, where a one-roll LSC was found to exist only for $Ra \lesssim 10^9$ to 10^{10}, and from measurements for $\Gamma = 0.5$ and $Pr \simeq 5$, where one- and two-roll structures were observed with transitions between them at random time intervals.

Key words: Bénard, convection

1. Introduction

Understanding turbulent Rayleigh–Bénard convection (RBC) in a fluid heated from below (Ahlers, Grossmann & Lohse 2009; Lohse & Xia, in press) remains a challenging problem in nonlinear physics. A major aspect is the global heat transport by the turbulent fluid. Another interesting feature of the dynamics of this system is a large-scale circulation (LSC). Apart from important applications in industry and astrophysics, the LSC provides an exciting example from fluid mechanics of systems that can be discussed in terms of non-equilibrium statistical mechanics (Brown & Ahlers 2006*a*, 2008).

Here we report results obtained with cylindrical samples of aspect ratio $\Gamma \equiv D/L \simeq 0.50$ (D is the diameter and L the height) as a function of the Rayleigh

† Email address for correspondence: guenter@physics.ucsb.edu

number $Ra = \alpha g \Delta T L^3/(\kappa\nu)$ over the range $10^7 \lesssim Ra \lesssim 10^{11}$ (α is the isobaric thermal expansion coefficient, g the acceleration of gravity, κ the thermal diffusivity, ν the kinematic viscosity and ΔT the applied temperature difference). We used helium gas at various pressures and at a mean temperature near ambient, where the Prandtl number $Pr \equiv \nu/\kappa$ is 0.674. We briefly report measurements of the Nusselt number $Nu = QL/(A\Delta T\lambda)$ (Q is the heat current passing through the sample, A the sample cross-sectional area and λ the thermal conductivity) and then focus on the properties of the LSC. For direct comparison we include new measurements and analyses for the case of $Pr = 4.38$, $\Gamma = 1.00$.

In the next section we describe three sample chambers, known as HPCF-I, HPCF-II and HPCF-III, that were used. In § 2.2 we explain how sidewall-temperature measurements were used to determine LSC properties. The results for Nu are presented in § 3.1. In § 3.2.1 we show results for the orientation and amplitude of the LSC as a function of time. Time-averaged statistical properties are presented in § 3.2.2. A brief summary is presented in § 4.

2. Apparatus and experimental methods

2.1. *The samples*

Three sample chambers, known as high-pressure convection facilities or HPCF, were used. Two of them (HPCF-I and HPCF-II) were of identical physical size with $L = 2240 \pm 2$ mm and $D = 1122 \pm 2$ mm, but HPCF-I had aluminium and HPCF-II had copper top and bottom plates. Each had a Plexiglas sidewall of thickness 0.95 cm and several isothermal shields that controlled stray heat currents. They were operated in a very large pressure chamber known as the 'Uboot of Göttingen' at the Max Planck Institute for Dynamics and Self-Organization in Göttingen, Germany. The Uboot of Göttingen is a cylinder, with a horizontal axis, of length 5 m and diameter 2.5 m. On top of it there is a turret of diameter 1.5 m and height 1.5 m, which can accommodate the full length of HPCF-I and HPCF-II. The Uboot can be filled with various gases, including helium, nitrogen and sulfur hexafluoride, at pressures of up to 19 bars. HPCF-III had $L = 490.0 \pm 0.5$ mm and $D = 246.6 \pm 0.3$ mm, an aluminium top plate and a copper bottom plate and a plexiglas sidewall of thickness 0.32 cm. It was operated in a pressure vessel of inner diameter 457 mm and height 914 mm located in our Santa Barbara laboratory. For each of the three sample chambers the bottom plate was a composite consisting of two metal plates with a layer of Lexan (polycarbonate) of thickness 5 mm between them. The plates extended a small distance, of the order of 1 cm, into the sidewall, and the sides facing the fluid had mirror finishes. Joule heating was applied uniformly to the bottom side of the composite. The heat current Q_s entering the sample was determined from the temperature drop across and the conductance of this composite (Malkus 1954; Krishnamurti & Howard 1981). The composite conductance was determined with an accuracy of about 1 %. Rayleigh numbers were determined from fluid properties evaluated at the mean temperature. The samples were helium gas (Prandtl number $Pr \equiv \nu/\kappa = 0.674$) at several pressures and near-ambient temperatures. Each data point was derived from a run of over 80 000 s, with the first 40 000 s discarded to avoid transients and the remainder averaged when appropriate.

For direct comparison, a more limited set of new results was obtained using water at 40°C where $Pr = 4.38$ in the 'medium apparatus' described by Brown *et al.* (2005*c*). That sample had $D = 247.8$ mm and $L = 247.8$ mm ($\Gamma = 1.00$), copper top and bottom plates, and a Plexiglas sidewall of thickness 3.2 mm.

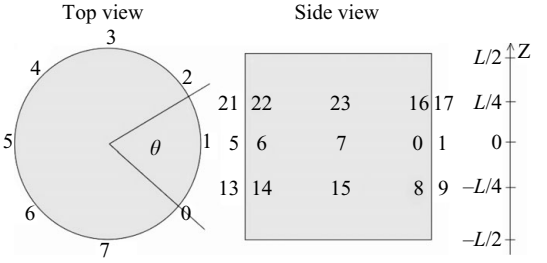

FIGURE 1. The location of the sidewall thermometers. For the top view, only the thermometer locations for the set located a distance $L/2$ above the bottom plate (on the horizontal mid-plane, or $z=0$) are shown. The side view indicates the location of all three sets. The z axis to the right of the side view shows the vertical location of the thermistor sets.

For comparison of the dynamics we mention that $\nu = 0.086\,\mathrm{cm^2\,s^{-1}}$ for helium at 30°C and 14.5 bars and $\nu = 6.7\times10^{-3}\,\mathrm{cm^2\,s^{-1}}$ for water at 40°C. This yields $t_v \equiv L^2/\nu = 5.8\times10^5$ (0.92×10^5) s for HPCF-I and HPCF-II (the medium apparatus). LSC turnover times τ_{LSC} depend on Ra and Pr as well as on the pressure. From the Reynolds-number results of Chavanne *et al.* (2001) we estimate roughly for HPCF-II that τ_{LSC} ranges from about 25 s near $Ra=10^9$ to 10 s near $Ra=10^{11}$. For comparison, $t_v \simeq 2\times10^5$ s for the $\Gamma=0.5$ samples of Xi & Xia (2007, 2008*a*,*b*) who obtained measurements for $1.6\times10^{10} \lesssim Ra \lesssim 7.2\times10^{10}$, with their longer runs at $Ra=5.7\times10^{10}$. For the $\Gamma=0.5$ sample of Xi & Xia (2007, 2008*a*,*b*) we estimate a turnover time at $Ra=1.6\times10^{10}$ (7.2×10^{10}) of 27 s (10 s). These values are not very different from those for our measurements with helium.

2.2. *Sidewall-temperature measurements*

Three sets of eight thermistors each, equally spaced around the circumference at the three vertical positions $-L/4$, 0 and $L/4$ (we take the origin of the vertical axis at the horizontal mid-plane of the sample) and labelled $i=0,\ldots,7$, and so on as shown in figure 1, were imbedded in small holes drilled horizontally into but not penetrating the sidewall (Brown, Nikolaenko & Ahlers 2005*b*; Ahlers, Brown & Nikolaenko 2006; Brown & Ahlers 2006*a*,*b*). The temperatures of all thermistors were measured with a sampling period of about 5s. Since the LSC carried warm (cold) fluid from the bottom (top) plate up (down) the sidewall, they detected the location of the upflow (downflow) of the LSC by being relatively high (low).

The orientation and strength of the LSC was determined by fitting the continuous function

$$T_f = T_{w,m} + \delta_m \cos(\theta_i - \theta_m), \quad i = 0,\ldots,7, \tag{2.1}$$

separately at each time step, to the eight temperature readings obtained from the thermistors at azimuthal position $\theta_i = i\pi/4$. The subscript 'm' indicates the vertical position at the horizontal mid-plane ($z=0$), and the subscript 'w' indicates that $T_{w,m}$ is measured at the sidewall. The three parameters $T_{w,m}$, δ_m and θ_m were least squares (LSQ) adjusted; δ_m is a measure of the temperature amplitude of the LSC, and θ_m is the azimuthal orientation of the plane of the LSC circulation. The azimuthal average of the temperature at the horizontal mid-plane is given by $T_{w,m}$. We calculated temperatures $T_{w,t}$ and $T_{w,b}$, orientations θ_t and θ_b and amplitudes δ_t and δ_b for the top and bottom levels at $z=L/4$ and $-L/4$ separately by the same method.

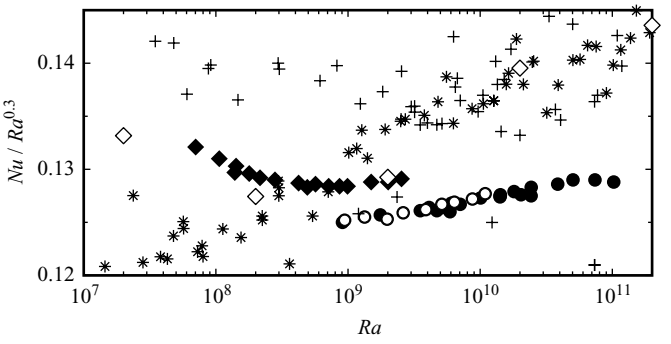

FIGURE 2. The reduced Nusselt number $Nu/Ra^{0.3}$ on a linear scale as a function of Ra on a logarithmic scale. Open circles: HPCF-I. Solid circles: HPCF-II. Solid diamonds: HPCF-III. Stars: from Niemela *et al.* (2000) as adjusted by Niemela & Sreenivasan (2006). Plus symbols: from Chavanne *et al.* (2001). Open diamonds: DNS for $Pr = 0.7$ (Stevens, Verzicco & Lohse, in press).

3. Results

3.1. *Nusselt numbers*

Results for Nu are plotted as $Nu/Ra^{0.3}$ in figure 2. The open (solid) circles are from HPCF-I (HPCF-II). They agree very well with each other, showing that end-plate corrections (Verzicco 2004; Brown *et al.* 2005*c*) are insignificant as expected. (Very recent measurements with SF_6 revealed that these corrections are quite small or negligible even for Ra as large as 10^{14}.) The solid diamonds are from HPCF-III. Where they overlap, they are about 2.5 % higher than the HPCF-I and HPCF-II results. This difference is within the estimates of systematic errors given in § 2.1. The data of Niemela *et al.* (2000; stars) are for $\Gamma = 0.50$ and $Pr = 0.69$. They generally are of the same size as ours but have a somewhat different Ra dependence. For small Ra (say $Ra \lesssim 10^9$) they have relatively large uncertainties because a significant and uncertain correction for the influence of the sidewalls (Ahlers 2000; Roche *et al.* 2001) on the heat flux through the sample had to be made (Niemela & Sreenivasan 2006). The results of Chavanne *et al.* (2001) are for slightly larger Pr (see e.g. figure 2 of Funfschilling, Bodenschatz & Ahlers 2009) and $\Gamma = 0.5$. They have a Ra dependence very similar to ours but on average are about 7 % higher. For further comparisons of various data, see also Funfschilling *et al.* (2009). The open diamonds are from direct numerical simulations (DNSs) by Stevens *et al.* (in press) for $Pr = 0.7$. At small Ra they agree well with our data. At larger Ra they are expected to be somewhat high because of inadequate spatial grid resolution.

3.2. *The large-scale circulation (LSC)*

3.2.1. *Time-dependent properties*

Unless explicitly stated, the data shown are for $Pr = 0.674$, $\Gamma = 0.50$, $Ra = 1.1 \times 10^{11}$, run 0906101 of HPCF-II, which extended over 1 70 000 s; but the behaviour of the LSC was found to be very similar at other Ra and for HPCF-III. It was not monitored during the HPCF-I measurements.

In figure 3(*a*) we show the three LSC orientations θ_k obtained by fitting (2.1) to the eight sidewall temperatures at any one time and separately at each of the three levels $k = b$, $k = m$ and $k = t$ (see figure 1). One sees that there are time intervals when the orientations are relatively steady, interspersed with time intervals of great and sudden change. The orientations at the three levels seem to differ from each other by

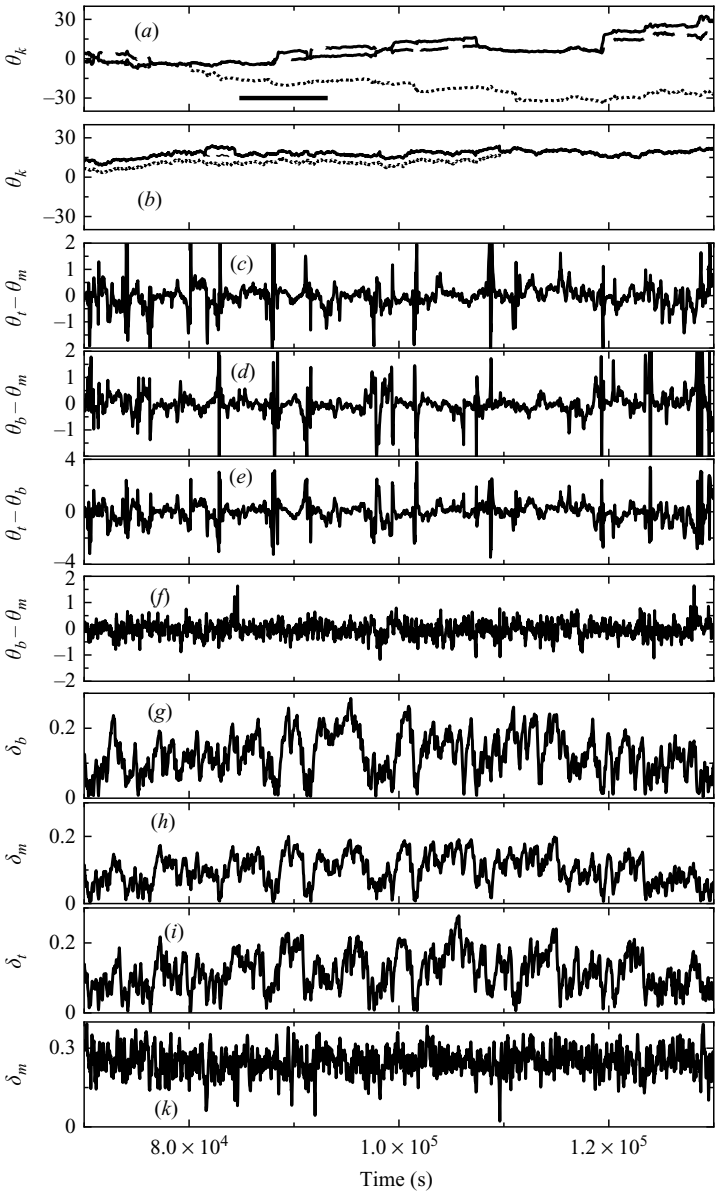

FIGURE 3. LSC dynamics. (*a*), (*c*)–(*e*), (*g*)–(*i*) From HPCF-II, run 0906101, $Pr = 0.674$, $\Gamma = 0.50$, $Ra = 1.0 \times 10^{11}$, $P = 15.50$ bars, $\Delta T = 28.4$ K. (*b*), (*f*), (*k*) From the medium apparatus, run 0907151, $Pr = 4.38$, $\Delta T = 20.00$ K, $\Gamma = 1.00$ and $Ra = 1.1 \times 10^{10}$. (*a*) The orientations θ_k, $k = b$ (solid line), $k = m$ (dashed line) and $k = t$ (dotted line). (Where the three lines can not be distinguished, two or three of them are on top of each other because the θ_k values are nearly the same.) (*b*) Analogous results to (*a*), but for $Pr = 4.38$. (*c*), (*d*) The difference $\theta_k - \theta_m$ for (*c*) $k = t$ and (*d*) $k = b$. (*e*) The difference $\theta_t - \theta_b$. (*f*) Analogous results to (*d*), but for $Pr = 4.38$. (*g*)–(*i*) The temperature amplitudes δ_k for (*g*) $k = b$, (*h*) $k = m$ and (*i*) $k = t$. (*k*) Analogous results to (*h*), but for $Pr = 4.38$, $\Gamma = 1.00$. All angles are in radians; all amplitudes δ are in Kelvin; and the origin of the time axis is at the beginning of the run.

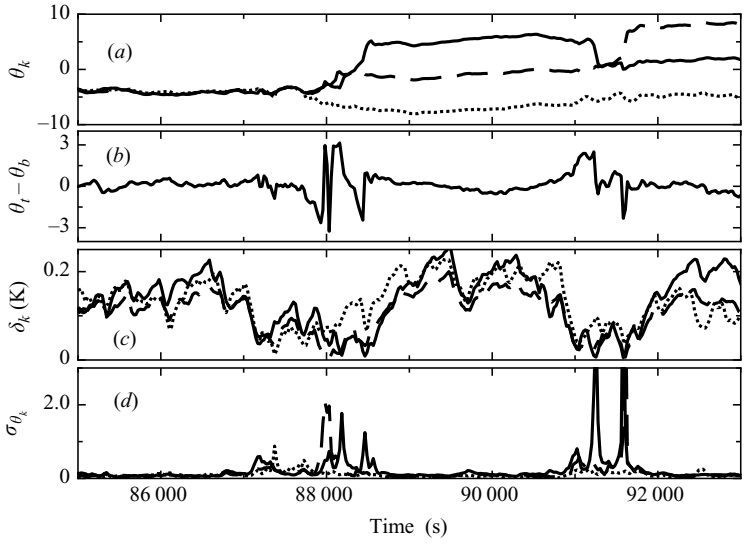

FIGURE 4. Details of LSC dynamics from figure 3, run 0906101, for $85\,000 \leqslant t \leqslant 93\,000$ s (the time interval indicated in (a) by the thick horizontal bar). (a) Orientations θ_k. (b) Differences $\theta_t - \theta_b$. (c) Temperature amplitudes δ_k. (d) Standard error σ_{θ_k} of θ_k. The lines in (a), (c) and (d) are as follows: the solid line is for $k = b$; the dashed line is for $k = m$; the dotted line is for $k = t$. Angles are in radians.

large amounts, but this is illusory, since the θ_k show the phase evolution of the LSC orientation and are 2π periodic; i.e. only θ mod 2π is relevant to the LSC orientation.

It is our view that the net rotations suggested by figure 3(a) can be a result of the LSQ analysis and may be unrelated to the physical rotation of the LSC circulation plane. In figure 4 we show detailed plots for the short time interval indicated by the horizontal solid line in figure 3(a). Figure 4(d) gives the probable error (67 % confidence limit) of θ_k derived from the fits. When δ_k (figure 4c) is small, an unambiguous fit cannot be obtained because there virtually is no signal, and the errors σ_{θ_k} of θ_k are large. In those cases very large unphysical changes of θ_k can be produced by the fitting procedure. This interpretation is consistent also with the results in figure 3(a), which indicate 'rotation' of the LSC plane in opposite directions at different levels rather than coherent rotation. Thus it is our interpretation that we have no evidence for the fast counterclockwise (when seen from above) average rotation, by a full revolution in an hour or two, nor for the fast instantaneous rotation (sometimes briefly at a rate of $20^\circ\,\mathrm{s}^{-1}$) that was reported by Sun, Xi & Xia (2005) for $\Gamma = 0.5$ and $Pr = 5.3$.

In figure 3(b) we show results that are analogous to those in figure 3(a) but for $Pr = 4.38$, $\Gamma = 1.00$ and $Ra = 1.1 \times 10^{10}$. One sees that the azimuthal displacements are much smaller and that the three levels tend to stay closer together. We note that for this case δ_k stays well above zero most of the time (see figure 3k), permitting an unambiguous LSQ fit almost all the time.

In figures 3(c)–3(e) we show $\theta_b - \theta_m$, $\theta_t - \theta_m$ and $\theta_t - \theta_b$, all shifted by multiples of 2π into the interval $\pm\pi$, as a function of time. There are periods when these quantities are close to zero, with only minor fluctuations of much less than a radian. During these intervals the LSC orientation is aligned at all three levels, indicating the existence of a single convection roll. These time intervals tend to coincide with those during which the orientations in figure 3(a) are relatively steady. Results for δ_k shown in figures 3(g)–3(i) indicate that the δ_k have relatively large values during these intervals

of coherent flow. Interspersed between these intervals are ones when the angular differences in figures 3(*c*)–3(*e*) become very large and erratic. These intervals tend to coincide with the ones in figure 3(*a*) when the orientations change rapidly and with the ones in figures 3(*g*)–3(*i*) when the δ_k are near zero; thus we believe that some or all of these large excursions are a result of the LSQ fitting procedure as explained above and that they do not correspond to any physical features of the LSC.

In figure 3(*f*) we show measurements that are analogous to those given in figure 3(*d*) but for $Pr = 4.38$, $\Gamma = 1.0$ (the results for $\theta_t - \theta_m$ are very similar). Here too the difference in orientation between the bottom ($z = -L/4$) and the middle ($z = 0$) hovers about zero, indicating the alignment expected from a single convection roll. There are very few large deviations. When these do occur, they are associated with cessations that involve a virtual vanishing of δ_k (see figure 3*k*). We note that during the periods of coherence the spread about $\theta_b - \theta_m = 0$ is larger for figure 3(*f*) than it is in figure 3(*d*). This is due to oscillations (unresolved on the time scale of the figure) associated with the torsional mode of the LSC for $\Gamma = 1$ (Funfschilling & Ahlers 2004; Funfschilling, Brown & Ahlers 2008; Xi & Xia 2008*a*), which were not observed for the $Pr = 0.674$, $\Gamma = 0.50$ case. (Indeed none were observed by Xi & Xia 2008*a* either for the $\Gamma \simeq 0.5$, $Pr \simeq 5$ case.) Our method of analysis could not reveal a sloshing mode (Zhou *et al.* 2009; Brown & Ahlers, in press), but that mode is likely to be absent as well for $\Gamma = 0.5$, since it is closely associated with the torsional mode.

We show the temperature amplitudes δ_k at the three levels in figures 3(*g*)–3(*i*). They vary widely with time, but they are roughly similar at the three levels at any one moment. This indicates that the LSC self-organizes into a substantial flow, coherent over the entire height of the cell, and then collapses again to a near-vanishing level. The intervals of great strength tend to coincide with those of relatively constant orientations in figure 3(*a*) and relatively small azimuthal differences in figures 3(*c*)–3(*e*). The periods of collapse typically have a duration of order 10^3 s. This is an order of magnitude longer than the typical duration of cessations as observed for $\Gamma = 1$, $Pr = 4.38$ (Brown & Ahlers 2006*b*) and $\Gamma = 0.5$, $Pr \simeq 5$ (Xi & Xia 2008*a*). This can be seen more clearly in figure 4(*c*). (In this connection it is noteworthy that the estimates of the turnover time of the LSC yield nearly the same values for the $Pr \simeq 5$, $\Gamma = 0.5$ case on the one hand and the $Pr = 0.674$, $\Gamma = 0.5$ case on the other because differences owing to the Pr and Ra dependencies of the Reynolds number are just about cancelled by the difference in the vertical viscous diffusion time of the two samples.) Thus we refrain from referring to the events for $Pr = 0.674$ as cessations.

An interesting question is whether these long-lasting and frequent collapses can be understood in terms of the model of Brown & Ahlers (2008) simply by changing the shape of the potential and the strength of the stochastic driving. In that case their physics is the same as that of cessations. But we cannot rule out that additional physics will have to be invoked at these smaller Prandtl numbers. A possibility is that lateral heat transport, which would be more important at small Pr, tends to overwhelm the LSC, as it does the Ekman vortices in rotating RBC (Zhong *et al.* 2009). In that case the collapses would be a qualitatively new phenomenon.

Finally, for comparison we show δ_m for $Pr = 4.38$, $\Gamma = 1.0$ in figure 3(*k*). In this case one sees that decays of δ_m close to zero, corresponding to cessations, are quite rare and, when they occur, are of very short duration.

The existence of a single role for $\Gamma = 1/2$ and $Pr \simeq 0.7$ was found also by DNS (Verzicco & Camussi 2003; Stringano & Verzicco 2006), but their work indicated a transition to a two-roll regime for Ra greater than 10^9 or 10^{10}. Up to $Ra \simeq 10^{11}$ we do not find such a transition.

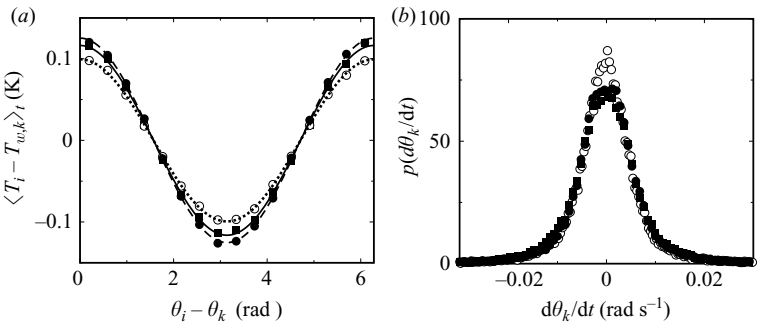

FIGURE 5. (*a*) The time-averaged azimuthal temperature variations $\langle T_i - T_{w,k}\rangle_t$ as a function of the azimuthal orientation $\theta_i - \theta_k$. The lines are fits of $\langle T_i - T_{w,k}\rangle = \langle \delta_k \rangle \cos(\theta_i - \theta_k)$ to the data, adjusting only $\langle \delta_k \rangle$, and correspond to $\langle \delta_t \rangle = 0.116$, $\langle \delta_m \rangle = 0.099$ and $\langle \delta_b \rangle = 0.125$. (*b*) The probability distributions of $d\theta_k/dt$. Solid circles: $k = b$. Open circles: $k = m$. Solid squares: $k = t$. Data are from run 0906101, HPCF-II.

Our observations of a single convection roll which spontaneously self-organizes and then collapses at irregular time intervals is different from the findings for $\Gamma = 0.5$ and $Pr \simeq 5$ by Xi & Xia (2008*b*). Those authors observed a sequence, irregular in time, of either a one-roll state or a state consisting of two rolls positioned approximately one above the other. Our data in figure 3 (and in all other runs) never gave an indication of the two-roll state, which would have led to a phase shift of π between θ_t and θ_b.

3.2.2. *Time-averaged properties*

In this section we examine several statistical (i.e. time-averaged) properties of the LSC.

An important question is whether the LSC produces the sinusoidal azimuthal temperature variation that is expected at the sidewall from a single convection roll. We show in figure 5(*a*) the time average $\langle T_i - T_{w,k}\rangle$, $k = b$, $k = m$ and $k = t$, as a function of $\theta_i - \theta_k$. Here both $T_{w,k}$ and θ_k were determined from fits of (2.1) to individual sets of eight temperatures, one each at the three vertical levels (see figure 1) and at each instant of time. Along the $(\theta_i - \theta_k)$ axis the data were first sorted into an arbitrarily chosen number of 16 bins and then time averaged separately in each bin. One sees that on average, the azimuthal temperature variation is well approximated by a cosine and that the amplitude, although slightly smaller at the horizontal mid-plane, is nearly the same at the three levels. The root-mean-square fluctuations of individual temperature readings about the fits of (2.1) to the data were typically about 20 % of $\langle \delta_k \rangle$. These findings are similar to what was reported for $Pr = 4.38$, $\Gamma = 1.00$. (Brown & Ahlers 2007)

The azimuthal dynamics is primarily diffusive, interrupted frequently by the collapses discussed in the previous section. It is characterized by typical rates of change $d\theta_k/dt$. Figure 5(*b*) gives the probability distributions of $d\theta_k/dt$. Typical absolute rates are less than 10^{-2} rad s^{-1}. One can infer that, for instance, $d\theta_m/dt < 0.024$ rad s^{-1} for 99 % of the run time. This differs from the case discussed by Sun *et al.* (2005), who reported larger rates.

In figure 6(*a*) we show the probability distribution of $\delta_k/\langle \delta_k \rangle$ (here $\langle \delta_k \rangle$ is the time average of δ_k). One sees that $p(\delta_k/\langle \delta_k \rangle)$ increases linearly with δ_k at small δ_k. This is very different from the results for $\Gamma = 1$, $Pr = 4.38$ shown in figure 6(*b*) and others reported previously, for instance those shown in figure 5 of Brown & Ahlers (2008). Those data revealed an exponential growth with δ_k at small δ_k. The exponential case is consistent with diffusion in a potential in the large-barrier limit;

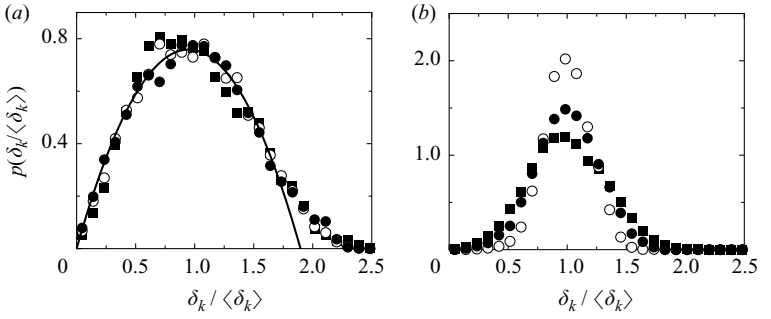

FIGURE 6. (*a*) The probability distribution of $\delta_k/\langle\delta_k\rangle$ for run 0906101, HPCF-II. The symbols are as in figure 5. The solid line is a fit of $p(\delta_k/\langle\delta_k\rangle) = a(\delta_k/\langle\delta_k\rangle) - b(\delta_k/\langle\delta_k\rangle)^2$ to the data for $k = m$ (middle row of thermistors) and $\delta_k/\langle\delta_k\rangle < 1.5$ which yielded $a = 1.60$ and $b = 0.84$. (*b*) Analogous results to (*a*), but for $Pr = 4.38$, $\Gamma = 1.00$ and $Ra = 1.1 \times 10^{10}$ (run 0907151, 'medium' apparatus).

the linear growth must be interpreted in terms of the more complicated case in which the barrier to diffusion is not large and in which the potential maximum at $\delta_k = 0$ is reached frequently. We also note that a Gaussian distribution about $\delta_k/\langle\delta_k\rangle = 1$, which is expected for diffusion in a deep potential and found in the $\Gamma = 1$, $Pr = 4.38$ case, is not a good approximation for $Pr = 0.674$, $\Gamma = 0.50$. Instead, the polynomial $p(\delta_k/\langle\delta_k\rangle) = a(\delta_k/\langle\delta_k\rangle) - b(\delta_k/\langle\delta_k\rangle)^2$ provides a good fit to the data up to $\delta_k/\langle\delta_k\rangle \simeq 1.5$ as shown in figure 6(*a*).

We note that integrating $p(\delta_k/\langle\delta_k\rangle)$ up to some cutoff value $(\delta_k/\langle\delta_k\rangle)_{cut}$ yields the fraction of time that the system spent with $\delta_k/\langle\delta_k\rangle$ below the cutoff. For example, $(\delta_k/\langle\delta_k\rangle)_{cut} = 0.2$ yields 3 % of the time for the case of figure 6(*a*) and 0.3 % for the case of figure 6(*b*).

Finally we remark that the results in figure 6(*a*), with the values of a and b close to 1.6 and 0.8 respectively, are typical for our entire range of Ra in both HPCF-II and HPCF-III.

4. Summary

The results for Nu differ somewhat from the previously reported data for $\Gamma = 0.5$ and similar Pr (Niemela *et al.* 2000; Chavanne *et al.* 2001; Niemela & Sreenivasan 2006), but the difference probably does not exceed the expected combined systematic errors. They are consistent with recent DNSs for this system (Stevens *et al.*, in press). These DNS data agree extremely well with our measurements at relatively small Ra but are higher than the experiment as Ra exceeds 10^9 or 10^{10}. According to Stevens *et al.* (in press) this difference at large Ra may be attributable to inadequate spatial grid resolution in the numerical work that is unavoidable, given the capabilities of current computers.

The results for the LSC are unexpected. Over the entire range of Ra the primary feature of the LSC is a single convection roll which, when it exists, is coherent along the entire length of the system. The DNS (Verzicco & Camussi 2003; Stringano & Verzicco 2006) had indicated that such a structure would be stable only for $Ra \lesssim 10^9$ to 10^{10}, whereas we find it all the way up to $Ra = 1.5 \times 10^{11}$.

For $\Gamma = 0.5$ and $Pr \simeq 5$ the LSC was studied extensively by Sun *et al.* (2005) and by Xi & Xia (2007, 2008*a*,*b*). Our results for $\Gamma = 0.5$ and $Pr = 0.674$ differ in interesting ways from theirs. Xi & Xia (2008*b*) found occasional transitions between a single

roll and two rolls, one above the other, with the two-roll state occurring on average about 7.9 % of the time. We have not observed this phenomenon in any of our runs; presumably it is absent for $Pr = 0.674$ and $Ra \lesssim 10^{11}$.

We also do not observe the net rotation at a mean rate of about 15 revolutions per day that was seen at larger Pr by Sun *et al.* (2005) and is revealed in figure 1 of their paper. Nor did we find the very large average instantaneous rates of $2.5^\circ\ s^{-1}$ cited by these authors. The maximum instantaneous rotation rate of $20^\circ\ s^{-1}$ ($0.35\,rad\,s^{-1}$) reported by them is outside the range of our $p(d\theta/dt)$ shown in figure 5(*b*) by more than an order of magnitude.

We find that the LSC organizes itself into a single roll of significant strength, coherent over the entire sample length, only to collapse again soon thereafter. This process of self-organization and collapse repeats at irregular time intervals, with the periods of weak or no flow occupying a significant fraction of the run time. The duration of the collapses typically is of order 10^3 s, which is an order of magnitude longer than the duration of cessations for $\Gamma = 1$, $Pr = 4.38$ (Brown, Funfschilling & Ahlers 2005*a*) and $\Gamma = 0.5$, $Pr \simeq 5$ (Xi & Xia 2008*a*).

We presented results for the probability distribution $p(\delta_k/\langle\delta_k\rangle)$ of the thermal flow amplitudes δ_k (here $\langle\delta_k\rangle$ is the time average of δ_k) at three vertical positions $k = b, m, t$ and showed that $p(\delta_k/\langle\delta_k\rangle)$ depends only slightly on vertical position. For $\Gamma = 1$, $Pr = 4.38$, $p(\delta_k/\langle\delta_k\rangle)$ grew exponentially with $\delta_k/\langle\delta_k\rangle$ at small $\delta_k/\langle\delta_k\rangle$; here we find that the representation $p(\delta_k/\langle\delta_k\rangle) = a(\delta_k/\langle\delta_k\rangle) - b(\delta_k/\langle\delta_k\rangle)^2$ provides a good fit to the results for $0 \leqslant \delta_k/\langle\delta_k\rangle \leqslant 1.5$.

In a recent model the LSC dynamics for $\Gamma = 1$ was described by diffusion in a potential well (Brown & Ahlers 2008), which, in a large-barrier approximation, leads to an exponential increase of $p(\delta_k)$ at small δ_k. Within the context of this model the linear increase of $p(\delta_k)$ at small δ_k implies that the large-barrier approximation is not valid in the present case. A detailed comparison with the model of all the current results is, unfortunately, well beyond the scope of this paper.

We are very grateful to the Max Planck Society and the Volkswagen Stiftung, whose generous support made the establishment of the facility and the experiments possible. The work of G.A. and J.H. was supported in part by the US National Science Foundation through grant DMR07-02111. We appreciate constructive comments from Heng-Dong Xi on an early version of this manuscript. We are very grateful to Artur Kubitzek and Andreas Renner for their enthusiastic technical support and to Holger Nobach for his role in developing the SF_6 system.

REFERENCES

Ahlers, G. 2000 Effect of sidewall conductance on heat-transport measurements for turbulent Rayleigh–Bénard convection. *Phys. Rev.* E **63**, 015303.

Ahlers, G., Brown, E. & Nikolaenko, A. 2006 The search for slow transients, and the effect of imperfect vertical alignment, in turbulent Rayleigh–Bénard convection. *J. Fluid Mech.* **557**, 347–367.

Ahlers, G., Grossmann, S. & Lohse, D. 2009 Heat transfer and large scale dynamics in turbulent Rayleigh–Bénard convection. *Rev. Mod. Phys.* **81**, 503–538.

Brown, E. & Ahlers, G. 2006*a* Effect of the Earth's Coriolis force on turbulent Rayleigh–Bénard convection in the laboratory. *Phys. Fluids* **18**, 125108-1–125108-15.

Brown, E. & Ahlers, G. 2006*b* Rotations and cessations of the large-scale circulation in turbulent Rayleigh–Bénard convection. *J. Fluid Mech.* **568**, 351–386.

Brown, E. & Ahlers, G. 2007 Temperature gradients, and search for non-Boussinesq effects, in the interior of turbulent Rayleigh–Bénard convection. *Europhys. Lett.* **80**, 14001-1–14001-6.

Brown, E. & Ahlers, G. 2008 A model of diffusion in a potential well for the dynamics of the large-scale circulation in turbulent Rayleigh–Bénard convection. *Phys. Fluids* **20**, 075101-1–075101-16.

Brown, E. & Ahlers, G. 2009 The origin of oscillations of the large-scale circulation of turbulent Rayleigh–Bénard convection. *J. Fluid Mech.* (in press).

Brown, E., Funfschilling, D. & Ahlers, G. 2005*a* Reorientation of the large-scale circulation in turbulent Rayleigh–Bénard convection. *Phys. Rev. Lett.* **95**, 084503.

Brown, E., Nikolaenko, A. & Ahlers, G. 2005*b* Reorientation of the large-scale circulation in turbulent Rayleigh–Bénard convection. *Phys. Rev. Lett.* **95**, 084503.

Brown, E., Nikolaenko, A., Funfschilling, D. & Ahlers, G. 2005*c* Heat transport by turbulent Rayleigh–Bénard convection: effect of finite top- and bottom-plate conductivity. *Phys. Fluids* **17**, 075108-1–075108-10.

Chavanne, X., Chilla, F., Chabaud, B., Castaing, B. & Hebral, B. 2001 Turbulent Rayleigh–Bénard convection in gaseous and liquid He. *Phys. Fluids* **13**, 1300–1320.

Funfschilling, D. & Ahlers, G. 2004 Plume motion and large scale circulation in a cylindrical Rayleigh–Bénard cell. *Phys. Rev. Lett.* **92**, 194502.

Funfschilling, D., Bodenschatz, E. & Ahlers, G. 2009 Search for the 'ultimate state' in turbulent Rayleigh–Bénard convection. *Phys. Rev. Lett.* **103**, 014503.

Funfschilling, D., Brown, E. & Ahlers, G. 2008 Torsional oscillations of the large-scale circulation in turbulent Rayleigh–Bénard convection. *J. Fluid Mech* **607**, 119–139.

Krishnamurti, R. & Howard, L. N. 1981 Large scale flow generation in turbulent convection. *Proc. Natl Acad. Sci.* **78**, 1981–1985.

Lohse, D. & Xia, K.-Q. 2010 Small-scale properties of turbulent Rayleigh–Bénard convection. *Annu. Rev. Fluid Mech.* (in press).

Malkus, M. V. R. 1954 The heat transport and spectrum of thermal turbulence. *Proc. R. Soc. London* A **225**, 196–212.

Niemela, J. J., Skrebek, L., Sreenivasan, K. R. & Donnelly, R. 2000 Turbulent convection at very high Rayleigh numbers. *Nature* **404**, 837–840.

Niemela, J. J. & Sreenivasan, K. R. 2006 The use of cryogenic helium for classical turbulence: promises and hurdles. *J. Low Temp. Phys.* **143**, 163–212.

Roche, P., Castaing, B., Chabaud, B., Hebral, B. & Sommeria, J. 2001 sidewall effects in Rayleigh–Bénard experiments. *Eur. Phys. J.* **24**, 405–408.

Stevens, R. J. A. M., Verzicco, R. & Lohse, D. 2009 Radial boundary-layer structure and Nusselt number in Rayleigh–Bénard convection. *J. Fluid Mech.* (in press), ArXiv: 0905.0379.

Stringano, G. & Verzicco, R. 2006 Mean flow structure in thermal convection in a cylindrical cell of aspect-ratio one half. *J. Fluid Mech.* **548**, 1–16.

Sun, C., Xi, H. D. & Xia, K. Q. 2005 Azimuthal symmetry, flow dynamics, and heat transport in turbulent thermal convection in a cylinder with an aspect ratio of 0.5. *Phys. Rev. Lett.* **95**, 074502.

Verzicco, R. 2004 Effect of non-perfect thermal sources in turbulent thermal convection. *Phys. Fluids* **16**, 1965–1979.

Verzicco, R. & Camussi, R. 2003 Numerical experiments on strongly turbulent thermal convection in a slender cylindrical cell. *J. Fluid Mech.* **477**, 19–49.

Xi, H.-D. & Xia, K.-Q. 2007 Cessations and reversals of the large-scale circulation in turbulent thermal convection. *Phys. Rev.* E **75**, 066307-1–066307-5.

Xi, H.-D. & Xia, K.-Q. 2008*a* Azimuthal motion, reorientation, cessation, and reversals of the large-scale circulation in turbulent thermal convection: a comparative study in aspect ratio one and one-half geometries. *Phys. Rev.* E **78**, 036326-1–036326-11.

Xi, H.-D. & Xia, K.-Q. 2008*b* Flow mode transition in turbulent thermal convection. *Phys. Fluids* **20**, 055104-1–055104-15.

Zhong, J.-Q., Stevens, R., Clercx, H., Verzicco, R., Lohse, D. & Ahlers, G. 2009 Prandtl-, Rayleigh-, and Rossby-number dependence of heat transport in turbulent rotating Rayleigh–Bénard convection. *Phys. Rev. Lett.* **102**, 044502-1–044502-4.

Zhou, Q., Xi, H.-D., Zhou, S.-Q., Sun, C. & Xia, K.-Q. 2009 Oscillations of the large-scale circulation in turbulent Rayleigh–Bénard convection: the sloshing mode and its relationship with the torsional mode. *J. Fluid Mech.* **630**, 367–390.